Damped Alfvén Waves in Bismuth: A Determination of Charge-Carrier Relaxation Times*

EDWIN H. MARSTON† AND YI-HAN KAO
Department of Physics, State University of New York, Stony Brook, New York 11790
(Received 11 July 1968; revised manuscript received 31 January 1969)

The average charge-carrier relaxation times in single-crystal bismuth at 4.2°K have been measured using a new technique. For Alfvén waves propagating in a slab of thickness d, the amplitude of Alfvén-wave oscillations increases with magnetic field B as $(V/c)e^{-d/V\tau}$, where V is the Alfvén-wave velocity proportional to B. Inasmuch as V can be determined from the standing-wave oscillations, our measurements of the amplitude growth in B provide us with a direct determination of the average relaxation time τ. We studied Alfvén-wave propagation along the three crystal axes using a resonant-cavity method in magnetic fields up to 11 kG. Strongly anisotropic relaxation times ranging from 0.15 to 0.40 nsec were obtained. The results are in good agreement with McLachlan's determination of the same quantities, but are in poor agreement with Brownell and Hygh's theory of Alfvén-wave damping. The experimental methods used here have several advantages over the usual galvanomagnetic and size-effect methods of determining τ. In addition, we predicted an interference effect in nonparallel-plate samples analogous to the Newton's-rings effect; this was borne out in our observations.

I. INTRODUCTION

THAT electromagnetic waves could propagate with small attenuation in certain stellar plasmas in the presence of a magnetic field was first proposed by Alfvén.[1] Buchsbaum and Galt[2] later suggested that this propagation mode—now called Alfvén waves—could also occur in solid-state plasmas. They interpreted the high magnetic field results of a microwave experiment by Galt *et al.*[3] and found good agreement with characteristic Alfvén-wave behavior. Observations of Alfvén-wave propagation in solids were later reported by several authors.[4–13]

Alfvén waves propagate only in materials having equal numbers of holes and electrons. To observe weakly damped Alfvén waves requires that the product of the average carrier relaxation time τ and the Alfvén frequency ω be greater than 1 ($\omega\tau>1$). In addition, the Alfvén frequency must be much less than the cyclotron frequency ω_c of the heaviest carrier.

Bismuth, which is a compensated semimetal belonging to group V of the Periodic Table, is a convenient solid-state plasma in which to study Alfvén waves. First, it has equal numbers of electrons and holes, since its carriers are due to the overlap of a filled valence band and an empty conduction band. Second, at 4.2°K scattering of carriers by phonons is essentially frozen out and the condition $\omega\tau>1$ is fulfilled at microwave frequencies. Third, the carrier effective masses in bismuth are much smaller than the free-electron mass, so that $\omega_c\gg\omega$ at low magnetic fields ($\sim$1 kG). Last, because of the stability of the carrier concentration in solids, the bismuth solid-state plasma can be used to study fundamental plasma dynamics.

Alfvén-wave propagation can also provide much information about bismuth itself. Several authors[5,9,12] have calculated the masses and concentrations of the bismuth carriers by measuring the Alfvén velocities for various crystal-axes–magnetic-field orientations.

The attenuation of Alfvén waves in bismuth has been studied in three experiments. Khaikin *et al.*[10] measured the Landau damping of Alfvén waves at microwave frequencies. Bartelink and Nordland[6] investigated Alfvén waves in the low-megacycle region. At these frequencies Alfvén waves are strongly damped, and their behavior is qualitatively different from that observed in the microwave region. McLachlan[13] studied lightly damped Alfvén waves from 200 to 3000 Mc/sec. In this frequency range $\omega\tau\sim1$ and the Alfvén velocity is a function of the frequency and relaxation times. By varying the frequency, McLachlan was able to obtain the average relaxation times.

In the present work, done in the 24-Gc/sec frequency range and at 4.2°K, the Alfvén velocity is frequency-independent. To determine the Alfvén damping, we derive in Sec. II an expression describing—as a function of magnetic field—the absorption of microwave power propagating as Alfvén waves in parallel-plate bismuth samples. From this expression, it is straightforward to obtain the power reflected from the sample surface,

* Based on part of a thesis submitted by Edwin H. Marston, in partial fulfillment of the requirements for the Ph.D. degree at the State University of New York at Stony Brook, 1968.

† Present address: Physics Department, Queens College, Flushing, N. Y. 11367.

[1] H. Alfvén, *Cosmical Electrodynamics* (Clarendon Press, Oxford, 1950).

[2] S. J. Buchsbaum and J. K. Galt, Phys. Fluids **4**, 1514 (1961).

[3] J. K. Galt, W. A. Yager, F. R. Merrit, B. B. Cetlin, and A. D. Brailsford, Phys. Rev. **114**, 1396 (1959).

[4] J. Kirsch and P. B. Miller, Phys. Rev. Letters **9**, 421 (1961).

[5] J. Kirsch, Phys. Rev. **133**, A1390 (1964).

[6] D. J. Bartelink and W. A. Nordland, Phys. Rev. **152**, 556 (1966).

[7] D. J. Bartelink, Bull. Am. Phys. Soc. Ser. II, **8**, 205 (1963).

[8] G. A. Williams and G. E. Smith, IBM J. Res. Develop. **8**, 276 (1964).

[9] G. A. Williams, Phys. Rev. **139**, A771 (1965).

[10] M. S. Khaikin, La Fal'kovskii, V. S. Edel'man, and R. T. Mina, Zh. Eksperim. i Teor. Fiz. **45**, 1704 (1963) [English transl.: Soviet Phys.—JETP **18**, 1167 (1964)].

[11] H. Kawamura, S. Nagata, T. Nakama, and S. Takano, Phys. Letters **15**, 111 (1965).

[12] B. W. Faughnan, J. Phys. Soc. Japan **20**, 574 (1965).

[13] D. S. McLachlan, Phys. Rev. **147**, 368 (1966).

which is the quantity we measured experimentally. The derived result relates the reflected power to the sample thickness, microwave frequency, Alfvén velocity, and an average relaxation time. The first four quantities can be directly measured, allowing the derived expression to be fitted to the relaxation time. Also derived in Sec. II is an expression describing Alfvén-wave propagation in non-parallel-plate samples. A strong modulation of the Alfvén-standing-wave pattern was predicted and observed.

Section III describes the experimental techniques and Sec. IV presents the results. Section V is a discussion of these results and the conclusion.

II. THEORY

In this section we wish to derive expressions describing the propagation of Alfvén waves in bismuth under the conditions of our experiment. The conditions are that B is in the plane of the parallel-plate sample, k is perpendicular to the sample surface, $\omega_c \gg \omega$, and $\omega\tau > 1$, where ω_c is the cyclotron frequency of the heaviest carrier, ω is the fixed microwave frequency, and τ is the average relaxation time.

Assuming plane-wave propagation in an isotropic solid-state plasma, we write

$$\mathbf{k}\times(\mathbf{k}\times\mathbf{E}) = -(4\pi i\omega/c^2)\mathbf{j} \tag{1}$$

and

$$\mathbf{j} = \boldsymbol{\sigma}(\mathbf{B})\cdot\mathbf{E}, \tag{2}$$

where $\mathbf{k}$ is the wave vector and $\boldsymbol{\sigma}(B)$ is the magnetoconductivity tensor. From (1) and (2)

$$\mathbf{k}(\mathbf{k}\cdot\mathbf{E}) - k^2\mathbf{E} + (4\pi i\omega/c^2)\boldsymbol{\sigma}(\mathbf{B})\cdot\mathbf{E} = 0. \tag{3}$$

We may derive the dispersion relation from this equation. For magnetic field $\mathbf{B}$ parallel to the z axis and in the plane of the sample and for k ($\|x$) perpendicular to the sample surface, Eq. (3) becomes

$$k^2 = (4\pi i\omega/c^2)(\sigma_{yy} - \sigma_{xy}\sigma_{yx}/\sigma_{xx}), \tag{4}$$

where the y axis is in the sample plane, and σ_{xz}, σ_{zx}, σ_{yz}, and σ_{zy} are taken to be zero.

Lax *et al.*,[14] assuming isotropic damping and a model of the bismuth Fermi surface consisting of three electron ellipsoids and one hole ellipsoid, have worked out the magnetoconductivity expressions for this material. In general, the conductivity tensor elements obtained are quite complicated. However, an examination of these elements for $\omega_c \gg \omega$ and B perpendicular to the microwave E field allows us to write Eq. (4) in the form

$$k^2 = \frac{\omega^2}{c^2}\frac{4\pi n f(m) c^2}{B^2}\left(1 + \frac{i}{\omega\tau}\right), \tag{5}$$

where $f(m)$ is a function of the effective masses. Using the results of Lax *et al.*, we list in Table I the $f(m)$ for the six field-axis configurations used in this experiment.

In the limit $\omega\tau \gg 1$, we obtain the propagation constant from (5):

$$\gamma = (\omega/V)(1 + i/2\omega\tau), \tag{6}$$

where V is the Alfvén velocity:

$$V = B/[4\pi n f(m)]^{1/2}.$$

For $\omega\tau \gg 1$, the wave propagates with little attenuation and V is independent of frequency and increases linearly with magnetic field.

To measure the Alfvén velocity, we use the fact that in a parallel-plate sample of thickness d, standing waves will occur when

$$d = l\lambda/2,$$

where l is an integer and λ is the Alfvén wavelength $2\pi V/\omega$. Assuming that the l standing wave occurs at B_1 and the $l+1$ standing wave at B_2, we have

$$l = (\omega d/\pi B_1)[4\pi n f(m)]^{1/2},$$
$$l+1 = (\omega d/\pi B_2)[4\pi n f(m)]^{1/2}.$$

Subtracting and rearranging yields

$$\Delta(1/B) = (\pi/\omega d)[4\pi n f(m)]^{-1/2}, \tag{7}$$

where

$$\Delta(1/B) = 1/B_2 - 1/B_1. \tag{8}$$

An experimental measurement of $\Delta(1/B)$ gives the real part of the propagation constant. In order to measure the imaginary part of γ, we must derive a relation between B and the power absorbed and reflected by the sample. We first match boundary condi-

TABLE I. Function $f(m)$ for various field-axis configurations. Here m_0 is the free-electron mass, the m's are the electron effective masses, and the M's are the hole effective masses. For details, see Refs. 14 and 16.

Sample	$k\|\|$, $B\|\|$, $E\|\|$	$f(m)$	$f(m)/m_0$	V (meas) 10^7B (kG) (cm/sec)	V (calc) 10^7B (kG) (cm/sec)
1	1, 2, 3	$\frac{1}{3}m_1 + (8/3)m_1m_2/(3m_1+m_2) + M_1$	0.088	5.73	5.85
1	1, 3, 2	$\frac{1}{2}(m_1+m_2) - \frac{1}{2}(m_4^2/m_3) + M_1$	0.403	2.48	2.73
2	2, 1, 3	$\frac{1}{3}m_2 + (8/3)m_1m_2/(m_1+3m_2) + M_2$	0.643	2.36	2.16
2	2, 3, 1	$\frac{1}{2}(m_1+m_2) - \frac{1}{2}(m_4^2/m_3) + M_2$	0.403	2.48	2.73
3	3, 1, 2	$m_3 - 2m_4^2/(m_1+3m_2) + M_3$	0.780	1.97	1.97
3	3, 2, 1	$m_3 - m_4^2/3m_2 - \frac{2}{3}m_4^2/(3m_1+m_2) + M_3$	0.774	1.87	1.97

[14] B. Lax, K. J. Button, H. J. Zeiger, and L. Roth, Phys. Rev. **102**, 715 (1956).

tions on both sides of a parallel-plate sample of thickness d and solve the equations for the ratio of the amplitudes of the incident ($\bar{A}$) and reflected ($\bar{B}$) waves:

$$\frac{\bar{B}}{\bar{A}}=\frac{(\omega^2/c^2-\gamma^2)(1-e^{2i\gamma d})}{(\omega/c+\gamma)^2-(\omega/c-\gamma)^2e^{2i\gamma d}}. \quad (9)$$

Assuming that $\omega\tau\gg1$ and $c/V\gg1$, Eq. (9) is solved for[15]

$$A=1-|\bar{B}/\bar{A}|^2,$$

where A is the sum of the power absorbed and transmitted by the sample; we obtained

$$A=D+\alpha(4V/c)[1+2\cos(4\pi d/\lambda)e^{-d/V\tau}], \quad (10)$$

where D and α are undetermined constants characteristic of the microwave system.

It is clear from Eq. (10) that the power entering the sample oscillates as $\cos(4\pi d/\lambda)$ because of geometric resonances. The expression also shows that the amplitude of the oscillations will increase with B. This amplitude growth is most easily analyzed by looking at the difference between the upper and lower oscillation envelopes. Setting $\cos(4\pi d/\lambda)=\pm1$, we have

$$A_+=D+\alpha(4V/c)(1+2e^{-d/V\tau}), \quad (11)$$

$$A_-=D+\alpha(4V/c)(1-2e^{-d/V\tau}). \quad (12)$$

Subtracting Eq. (12) from Eq. (11) gives the oscillation envelope amplitude:

$$E=16\alpha(V/c)e^{-d/V\tau}. \quad (13)$$

Using Eq. (13), the fact that the detection system output is directly proportional to the power absorbed and transmitted by the sample, and the determination of the Alfvén velocity from $\Delta(1/B)$, it is possible to measure the average relaxation times.

The above results were derived for parallel-plate samples. In our frequency and magnetic field range, the Alfvén wavelength is on the order of 0.002 cm. It is therefore of interest to see what effects arise in a sample with nonparallel surfaces. To investigate the domain where the variation in thickness Δd is about an Alfvén wavelength, we average the oscillatory term in Eq. (10):

$$A'=\alpha\frac{8V}{c\Delta d}\int_d^{d+\Delta d}\cos\left(\frac{4\pi x}{\lambda}\right)e^{-x/V\tau}dx, \quad (14)$$

where d is the thickness at one end of the sample and $d+\Delta d$ is the thickness at the other. Carrying out the integration and dropping small terms yields

$$A'=\alpha\frac{8V}{c}\cos\left(\frac{4\pi d}{\lambda}\right)e^{-d/V\tau}\frac{\sin(2\pi\Delta d/\lambda)}{2\pi\Delta d/\lambda}. \quad (15)$$

This expression predicts that the fast oscillations—periodic in $4\pi d/\lambda$—will be modulated by slow oscillations—periodic in $2\pi\Delta d/\lambda$—as B increases. The ratio of the periods will go as $2d/\Delta d$.

[15] Edwin H. Marston and Y. H. Kao, Physik Kondensierten Materie 9, 195 (1969).

III. EXPERIMENTAL TECHNIQUES

A. Sample Preparation

The three parallel-face bismuth samples used were all spark-cut from the center of a single-crystal ingot 15 cm long. The crystal was grown from commercially obtained 99.9999%-pure bismuth by zone leveling. Zone leveling was used so that the three samples would have a uniform impurity content.

Each sample was approximately 1×1×0.2 cm with a principal axis perpendicular to the surface. The samples were oriented with an accuracy of 1° by back-reflection Laue photography. After cutting and orienting, the sample surfaces were chemically polished in a solution of six parts glacial acetic acid, six parts fuming nitric acid, and one part distilled water.

B. Microwave Spectrometer

During the runs, a sample was placed over a hole in the bottom wall of a rectangular, silver-plated microwave cavity resonating at 24 Gc/sec in the TE102 mode. The sample was aligned on the cavity by eye and was subject to an error of 2°. The cavity, sample, and associated waveguide were then placed in a Sulfrian stainless-steel Dewar whose tail was between the pole faces of a 12-in. Magnion electromagnet mounted on a rotatable base. With this geometry, the magnetic field was always parallel to the sample surface and could be rotated from B parallel to E_{rf} to B perpendicular to E_{rf}. All data were taken at 4.2°K and in fields up to 11 kG.

Microwave power was coupled into the cavity through a round iris between the cavity and waveguide. An adjustable screw set into the waveguide near the iris permitted fine adjustments in the coupling. Most runs were made with the cavity undercoupled, approximately 15% from the critically coupled position.

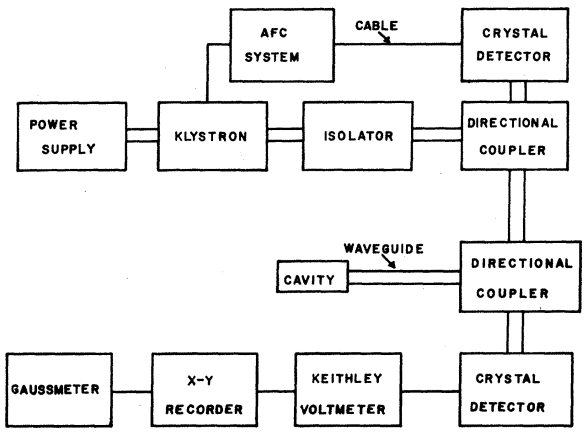

FIG. 1. Block diagram of the microwave system.

Figure 1 is a schematic of the microwave spectrometer. Power reflected from the cavity caused a dc voltage in the crystal detector. The voltage was fed into a Keithley 150AR milli-microvoltmeter whose output drove the Y axis of a Varian F-80 X-Y recorder. The X axis of the recorder was driven by the output of a Bell 240 Hall probe gaussmeter which measured the magnetic field at the sample.

Because the short-term drift of the klystron was comparable to the cavity resonance width, it was necessary to use an automatic frequency control (AFC) system. The AFC consisted of an oscillator which modulated the cavity resonance at 10 kc/sec and a phase-sensitive detector tuned to 10 kc/sec to monitor the power reflected from the cavity. As long as the klystron was centered on the cavity resonance, the 10-kc/sec modulation resulted in a pure 20-kc/sec modulation of the power reflected from the cavity. But if the microwave frequency drifted off the cavity resonance, some 10-kc/sec signal would be mixed in. The phase-sensitive detector would then apply a correction voltage to the klystron's repeller, pushing it back on resonance.

C. Detection Characteristics

If the crystal detector is operated in the square-law region, then

$$\Delta P_r \propto \Delta V_{\text{xtal}},$$

where ΔP_r is the change in power reflected from the cavity and ΔV_{xtal} is the change in detector voltage. It can also be shown that in the square-law region for small changes in the sample surface resistance ΔR_s

$$\Delta P_r \propto -\Delta Q \propto \Delta R_s, \tag{16}$$

where Q is proportional to the ratio of the power stored to the power lost in the cavity and R_s is the cavity surface resistance. Background runs on the cavity without the sample showed no change in the reflected power as B was swept, so all observed changes were attributed to the sample. Therefore, changes in crystal detector voltage were directly proportional to the surface resistance of the sample, which in turn was directly proportional to changes in the power absorbed or transmitted by the sample. This was convenient, since the quantity A in Eq. (10) was directly proportional to the crystal detector voltage.

IV. EXPERIMENTAL RESULTS AND ANALYSIS

A typical experimental curve is shown in Fig. 2. An X-Y recorder plotted the magnetic field (X axis) versus the crystal detector voltage (Y axis), which was proportional to the sample surface resistance. All data were taken at 4.2°K with E_{rf} and B in the plane of the sample.

The Alfvén velocity was obtained for each of the six field–crystal-axes configurations as listed in Table I by plotting the $1/B$ values of the oscillation maxima (or minima) versus the fringe index. Figure 3 is a typical plot of l versus $1/B$ with the points fitted to a straight line. The slope is

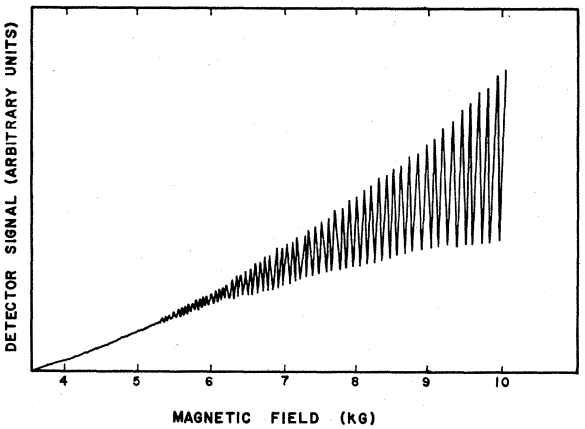

FIG. 2. Typical standing-wave oscillations with k parallel to the bisectrix axis and E_{rf} parallel to the trigonal axis in sample 2 at 24.2 Gc/sec. The amplitude grows with B. The curve also shows the Shubnikov–de Haas modulation of the oscillations.

$$\frac{\Delta l}{\Delta(1/B)} = \frac{\omega d}{\pi}[4\pi n f(m)]^{1/2}. \tag{17}$$

The six measured Alfvén velocities are listed in Table I along with their theoretical values. The latter were calculated using the conductivity tensor derived

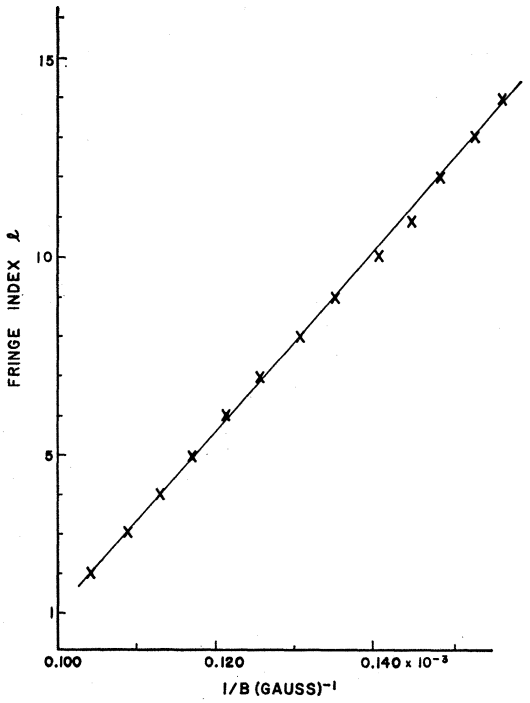

FIG. 3. Typical plot of l versus $1/B$. k is parallel to the binary axis and E_{rf} to the trigonal axis. The errors are the size of the X's.

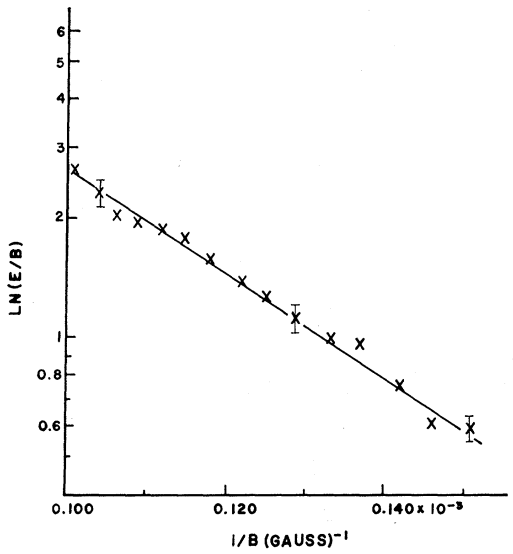

FIG. 4. Semilog plot of $1/B$ versus E/B, where E is the oscillation envelope, for sample 2. k is parallel to the bisectrix axis, B to the trigonal axis, and E_{rf} to the binary axis.

by Lax *et al.*,[14] Kao's[16] effective-mass values, and Bhargava's[17] value for the carrier concentration. Agreement is good except for the second and fourth configurations, where the m_4 term is important. These two orientations are very sensitive to the crystal field directions and the discrepancies are probably due to misalignment.

An inspection of the X-Y plots shows that the oscillation amplitude grows with increasing magnetic field. This growth is predicted by the expression derived in Sec. II [Eq. (13)]. To measure E, the amplitude of the oscillation envelope, we drew in on the X-Y plot the upper and lower envelopes and measured the separation at 200-G intervals. To use these data it is convenient to rewrite Eq. (13) as

$$E=\alpha\frac{16B}{c[4\pi nf(m)]^{1/2}}\exp\left(-\frac{d[4\pi nf(m)]^{1/2}}{B\tau}\right). \quad (18)$$

Rearranging and taking the natural log of both sides yields

$$\ln\frac{E}{B}=\ln\frac{16\alpha}{c[4\pi nf(m)]^{1/2}}-\frac{d[4\pi nf(m)]^{1/2}}{B\tau}. \quad (19)$$

If E/B is now plotted versus $1/B$ on a semilog scale and the points fitted to a straight line, the slope of the line is

$$S=\frac{\ln E/B}{1/B}=-\frac{d[4\pi nf(m)]^{1/2}}{\tau}. \quad (20)$$

Since $[4\pi nf(m)]^{1/2}$ is known from the velocity measurements, the slope gives the relaxation time.

Figures 4 and 5 are semilog plots of E/B versus $1/B$. The large oscillations about the straight line are due to the presence of the Shubnikov–de Haas effect. This effect, which is periodic in $1/B$, is due to a variation of the carrier scattering time. The "error limits" are the approximate variation in the relaxation time due to the magnetic field dependence of τ.

The measured relaxation times are listed in Table II, along with McLachlan's values of τ.[13] The first six τ's in Table II are those determined using the three samples prepared from the center section of the zone-leveled ingot. The seventh relaxation time (1′) was obtained from sample 1 after it was reduced in thickness by 0.020 in. and the surface repolished. The eighth and

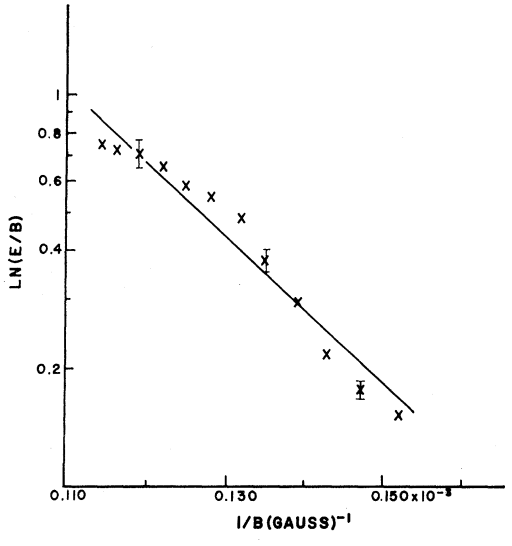

FIG. 5. Semilog plot of $1/B$ versus E/B, where E is the oscillation envelope for sample 1. k is parallel to the binary axis, B to the bisectrix axis, and E_{rf} to the trigonal axis.

[16] Y. H. Kao, Phys. Rev. **129**, 1122 (1963).
[17] R. N. Bhargava, Phys. Rev. **156**, 785 (1967).

TABLE II. Relaxation times.

Sample	$k\|\|$, $B\|\|$, $E\|\|$	ν (Gc/sec)	τ (nsec) This work	τ (nsec) McLachlan
1	1, 2, 3	24	0.13 (0.17–0.09)	0.15 (0.17–0.12)
1	1, 3, 2	24	0.31 (0.34–0.28)	0.22 (0.27–0.18)
2	2, 1, 3	24	0.38 (0.42–0.34)	0.55 (1.0 –0.35)
2	2, 3, 1	24	0.40 (0.44–0.36)	0.27 (0.34–0.23)
3	3, 1, 2	24	0.20 (0.22–0.18)	0.21 (0.24–0.18)
3	3, 2, 1	24	0.35 (0.43–0.27)	0.37 (0.50–0.28)
1′	1, 2, 3	24	0.15 (0.20–0.10)	0.15 (0.17–0.12)
4	1, 3, 2	9	0.35 (0.38–0.32)	0.22 (0.27–0.18)
5	3, 1, 2	24	0.14 (0.16–0.12)	0.21 (0.24–0.18)

ninth values were obtained on samples 4 and 5 prepared from different ingots and one run was made at 9.0 rather than 24.15 Gc/sec.

As can be seen from Table II, the last three relaxation times are in good agreement with the corresponding relaxation times among the first six. This shows that the values are not strong functions of the surface condition or of the particular crystal on which the measurement was made. The agreement with four of the six relaxation times measured by McLachlan is also good. The two values for which there is disagreement are for the second and fourth field-axis configurations for which, according to McLachlan, his method of determining τ is subject to errors of up to 30%.

In Sec. II, we derived Eq. (15), which predicts that the effect of a nonparallel-plate sample would be to modulate the growth of Alfvén oscillations according to

$$\cos\left(\frac{4\pi d}{\lambda}\right)\frac{\sin(2\pi\Delta d/\lambda)}{2\pi\Delta d/\lambda}, \qquad (21)$$

where small terms have been dropped.

To test this prediction, data were taken on parallel-plate sample 4. The sample was then spark-planed so that $d/\Delta d\cong 25$. In the parallel-plate state (Fig. 6), no modulation was observed, but in the nonparallel state, with the same crystal-axis–field orientation, a strong modulation was seen, as shown in Fig. 7.

To evaluate Eq. (21) quantitatively, we relate $d/\Delta d$ to the number of oscillations between adjacent modulation minima. In a full cycle we expect

$$\text{No. of peaks} = 2d/\Delta d \simeq 50.$$

In Fig. 7, there are approximately 28 peaks between the two minima, corresponding to 56 peaks in a full cycle. The agreement is reasonably good, considering the uncertainty in the exact position of the minima and the variation of the microwave fields over the sample surface.

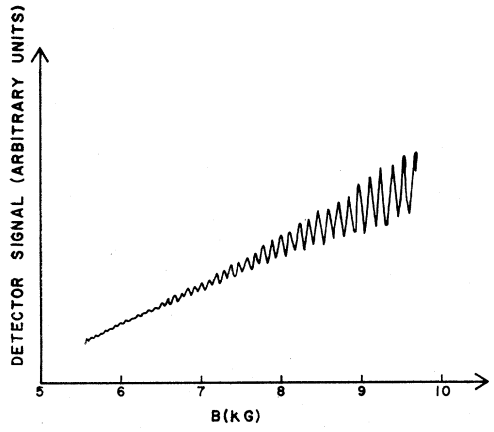

FIG. 6. Sample 2 in the parallel-face state with E parallel to the binary axis and B parallel to the trigonal axis.

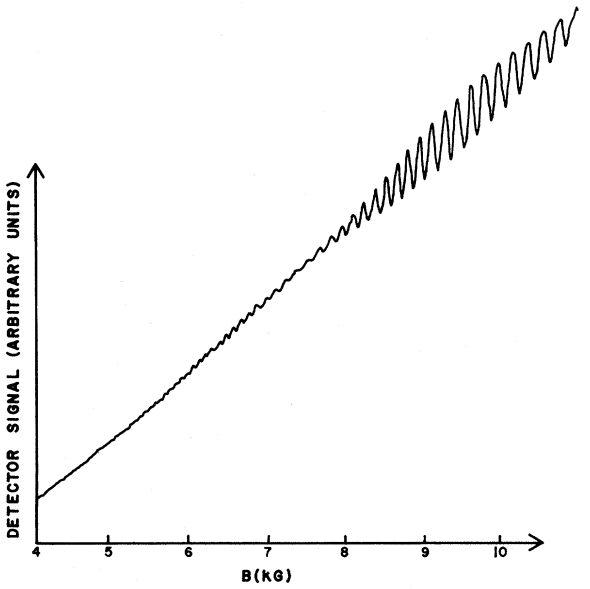

FIG. 7. Sample 2 in the nonparallel state. E is parallel to the binary axis, B parallel to the trigonal axis.

This interference effect can be thought of as a dynamic observation of Newton's rings. In the optical Newton's-rings effect, a standing-wave interference pattern is formed by two nonparallel reflecting surfaces. In the present situation, the interference pattern is integrated over rather than scanned across. Then, as λ increases, the number of fringes in the sample decreases, causing the integrated interference pattern to oscillate in intensity.

V. DISCUSSION

At 4.2°K, if lattice vibrations are frozen out, the possible relaxation mechanisms are impurity or defect scattering and electron-electron scattering. Assuming that electron-electron scattering is the dominant mechanism, then the relaxation time should vary as T^2.[18] We attempted to determine the temperature dependence, but the rapid growth of the Shubnikov–de Haas effect below 4.2°K and the loss of sensitivity at higher temperatures prevented an accurate measurement.

Assuming ionized impurity or defect scattering, Brownell and Hygh[19] have calculated the ratios of the relaxation times measured in this experiment. Figure 8, which compares their predictions with our data, shows that the agreement is not good. They stated that to fit their results to McLachlan's data required the concentration of ionized impurities to be 4.2% of the electron or hole concentration. However, an impurity concentration of this size would make the sample too uncompensated for Alfvén-wave propagation. Brownell and Hygh therefore suggested that Frenkel defects could

[18] J. M. Ziman, *Electrons and Phonons* (Oxford University Press, New York, 1960).

[19] D. H. Brownell, Jr., and E. H. Hygh, Phys. Rev. **164**, 916 (1967).

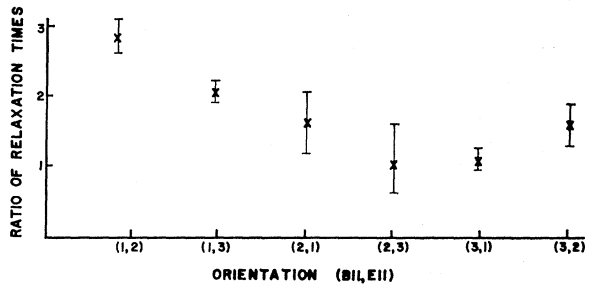

FIG. 8. Normalized ratios of the theoretical relaxation times calculated by Brownell and Hygh to our experimental values. On the X axis, the first number in parentheses refers to the B field direction and the second to the E_{rf} field direction. The binary axis is 1, bisectrix axis 2, and trigonal axis 3. The ratio at (2,3) was taken to be 1.

provide the required percentage of scattering centers and yet preserve electron-hole equality. But the Frenkel defect concentration is sensitive to the prior history of the sample, and we would expect different samples to give different results, especially those prepared in different ways or cycled from room temperature to 4.2°K a different number of times. The good internal agreement in the present experiment and the agreement between our results and McLachlan's results imply that the cause of the relaxation-time values is probably not Frenkel defects.

The present experimental technique is very convenient in comparison with the size-effect and galvanomagnetic[20] methods of determining the relaxation times. In the size-effect method, the resistance is measured in samples at different thicknesses, allowing a determination of $d/V_F\tau$ (where V_F is the Fermi velocity). However, the frequent thermal cycling and the possible strains and dislocations introduced in reducing the size of an already very thin sample make the method subject to error. In the present method, $e^{-d/V\tau}$ is determined in a single sample with one sweep of the magnetic field. In comparison with galvanomagnetic methods, no assumption is made about the Fermi-surface model and no leads are attached to the sample in the present work; thus, it should give a more direct determination of the relaxation times.

ACKNOWLEDGMENTS

We would like to thank Jay Kirschenbaum for his help in the microwave work, and B. Sutherland for useful discussions.

[20] R. N. Zitter, Phys. Rev. **127**, 1471 (1962).

PHYSICAL REVIEW VOLUME 182, NUMBER 2 10 JUNE 1969

Raman Scattering from Solid-State Plasmas

P. M. PLATZMAN
Bell Telephone Laboratories, Murray Hill, New Jersey 07974

AND

N. TZOAR
The City College of The City University of New York, New York, New York 10031

(Received 2 April 1968; revised manuscript received 10 January 1969)

A microscopic calculation of the Raman scattering process in almost transparent semiconductors is presented. The calculation takes into account band structure, phonons, and the collective motions of the conduction electrons. It is based on many-body perturbation theory and is "valid" within the framework of the random-phase approximation. Our results show resonance scattering from the coupled collective modes of the conduction-electron longitudinal-optic-mode system. The detailed effect of the band structure manifests itself in determining the intensity of the resonance lines.

I. INTRODUCTION

THE ever increasing availability of intense monochromatic sources in the infrared has made possible Raman scattering from narrow-band-gap semiconductors. More specifically, successful light scattering experiments have been performed in weakly doped GaAs,[1] InAs, and InSb.[2] An analysis of the data in these three experiments has been based on rather simple theoretical treatment of the light scattering problem.[3,4] The theory is essentially formulated in terms of a single-band model of a semiconductor. The band structure is assumed to be completely characterized by an effective-mass tensor and sometimes by an additional enhancement factor which in an approximate way

[1] A. Mooradian and G. B. Wright, Phys. Rev. Letters **16**, 999 (1966).

[2] R. E. Slusher, C. K. N. Patel, and P. A. Fleury, Phys. Rev. Letters **18**, 530 (1967); C. K. N. Patel and R. E. Slusher, Phys. Rev. (to be published).

[3] P. M. Platzman, Phys. Rev. **139**, A379 (1965); A. L. McWhorter, in *Physics of Quantum Electronics*, edited by P. L. Kelley, B. Lax, and P. E. Tannenwald (McGraw-Hill Book Co., New York, 1966), p. 111.

[4] Y. C. Lee and N. Tzoar, Phys. Rev. **140**, A396 (1965).